# Information of Electromagnetic Scattering and Radiative Transfer in Natural Media

## Volume 2 (2001–2010)

Jin Ya-Qiu

Science Press
Beijing, China

# Information of Electromagnetic Scattering and Radiative Transfer in Natural Media

## Volume 2 (2001—2010)

Jin Ya-Qiu



SCIENCE PRESS
Beijing, China

*Responsible Editor*: *Peng Shengchao*


Published by Science Press
16 Donghuangchenggen North Street
Beijing 100717, China

Printed in Beijing



ISBN 978-7-03-031225-9 (Beijing)
RMB: 280.00

# Author

**Jin Ya-Qiu** graduated from Peking University, Beijing, China in 1970, and received the M. S. , E. E. , and Ph. D. degrees from the Massachusetts Institute of Technology, Cambridge, USA in 1982, 1983 and 1985, respectively. All the degrees are from electrical engineering.

He was a Research Scientist with the Atmospheric and Environmental Research, Inc. , Cambridge MA, USA (1985); a Research Associate with the City University of New York (1986-1987); a Visiting Professor with the University of York, U. K. (1993-1994) sponsored by the U. K. Royal Society; a Visiting Professor with the City University of Hong Kong (2001); and a Visiting Professor with Tohoku University, Japan (2005). He held the Senior Research Associateship at NOAA/NESDIS awarded by the USA National Research Council (1996). He is currently a Chair Professor of Fudan University, Shanghai, China, and the founder Director of the Key Laboratory of Wave Scattering and Remote Sensing Information (MoE, Ministry of Education). He has been appointed as the Principal Scientist for the China State Key Basic Research Project (2001-2006) by the Ministry of National Science and Technology of China to lead the remote sensing program in China.

He has published more than 620 papers in refereed journals and conference proceedings and 12 books, including *Electromagnetic Scattering Modeling for Quantitative Remote Sensing* (World Scientific, 1994), *Information of Electromagnetic Scattering and Radiative Transfer in Natural Media First volume* 1983-2000 (Science Press, 2000), *Theory and Approach for Information Retrieval from Electromagnetic Scattering and Remote Sensing* (Springer, 2005)]. He is Editor of *Wave Propagation, Scattering and Emission in Complex Media* (World Scientific and Science Press, 2004) and Co-Editor of the book *Selected Papers on Microwave Lunar Exploration in Chinese Chang'E-1 Project*(Science Press, 2011) and SPIE Volume 3503 *Microwave Remote Sensing of the Atmosphere and Environment*.

His main research interests include scattering and radiative transfer in complex natural media, microwave remote sensing, as well as theoretical modeling, information retrieval and applications for atmosphere, ocean, and earth terrain surfaces, and computational electromagnetics.

Dr. Jin is the IEEE Fellow for his contributions of electromagnetic scattering model for remote sensing applications, the member of IEEE GRSS AdCom, Chair of IEEE Fellow Evaluation Committee in GRSS, IEEE GRSS Distinguished Speaker, and an Associate Editor of IEEE Transactions on Geoscience and Remote Sensing. He is also the Fellow of Electromagnetics Academy (USA) and CIE. He received IEEE GRSS Education Award (2010) in recognition of his significant educational contributions to geoscience and remote sensing.

He is Co-Chair of Technical Committee of IGARSS2011, ISAPE2000 and 2010, and Chair of JURSE2009 and several international conferences. He is the Founder Chairman of IEEE GRSS Beijing Chapter (1998-2003) and received the appreciation for his notable service and contributions toward the advancement of IEEE professions from IEEE GRSS.

He received the China National Science Prize in 1993, the first-grade Science Prizes of MoE in 1992, 1996 and 2009, and the first-grade Guang-Hua Science Prize in 1993 among many other prizes.

# 作者简介

金亚秋1970年毕业于北京大学，1978年为中国科学院首批公派出国研究生，分别于1982年、1983年、1985年2月获美国麻省理工学院(MIT)电气工程与计算机科学系(EECS)科学硕士(MS)、电气工程师(EE)、博士(Ph. D.)学位。曾先后任职于美国大气环境研究公司(AER)、美国纽约市立大学(CUNY)、英国约克大学(U. York)、美国国家海洋大气局卫星研究室(NOAA/NESDIS)、香港城市大学(CUHK)、日本东北大学(Tohoku U)。现任复旦大学特聘教授、波散射与遥感信息教育部重点实验室主任。

他是国家重点基础研究973项目“复杂自然环境时空定量信息获取与融合处理的理论与应用”(2001CB309400)首席科学家，国家级有突出贡献的中青年科技专家、国家自然科学基金会首次十位优秀中青年人才基金(国家杰出青年基金前身)获得者、上海市劳动模范、IEEE GRSS北京支会创始主席(1998—2003)，中国电子学会微波遥感与无线电遥感、中国计算物理学会计算电磁三个专业委员会创始主席、国家教育部电子科学与技术分教学指导委员会副主任委员(2000—2010)。

他是中国与发展中国家在遥感(IEEE GRSS，Geoscience and Remote Sensing Society)领域第一个IEEE Fellow，第一位IEEE GRSS AdCom委员，IEEE Fellow评选委员会主席(GRSS)、IEEE GRS杰出演讲者，任IEEE Transactions on Geoscience and Remote Sensing副主编。他也是美国电磁研究院(EMA)Fellow与CIE Fellow。他获得IEEE GRSS Education Award(教育奖)(2010)。并任国际学术会议Urban Joint Event on Remote Sensing主席(2009)、ISAPE(2000、2010)、IGARSS(2011)技术委员会主席等。

他的研究领域为复杂自然环境中电磁波散射辐射传输与传播、空间遥感与对地监测信息理论与技术、复杂系统中计算电磁学等。他在国内外已发表620多篇学术论文、12本中英文专著与文集。

他曾获国家自然科学奖三等奖(1993)、三次国家教育部自然科学奖一等奖(1992，1996，2009)、光华科技奖一等奖(1993)、国家图书奖(1997)、全国科技图书奖一等奖(1997)、首届全国宝钢教育基金优秀教师特等奖(1994)、上海市科技进步奖(2000)与国家教育部自然科学奖二等奖(1999)各一次、国家973计划先进个人(2004)等十多项科技奖励，是复旦大学首届优秀研究生导师、复旦大学校长奖、上海市优秀教学奖，两届上海市十大科技精英与首届上海市十大高校精英提名奖获得者。他主持承担国家与部市委四十多项重大、重点项目，他至今完成的六项国家自然科学基金信息项目评为特优。

# Preface

This book is the second volume of selected journal papers of my publications during 2001-2010. The first volume of the selected journal papers during 1983-2000 was published by Science Press in 2000. These two volumes represent my main research works on electromagnetitic scattering, radiative transfer and space-borne microwave remote sensing during three decades. Especially, this second volume collected my works when I was appointed as the Principle Scientist of the state major basic research (973) project (2001CB309400) in 2000-2006 by the State Ministry of Science and Technology of China.

The polarimetric imagery of synthetic aperture radar (POL-SAR) technology is one of most important advances in space-borne microwave remote sensing during recent decades. Part 1 deals with fully polarimetric scattering theory and information retrieval from POL-SAR images. The parameterized model of random non-spherical scatter media and Mueller matrix solution are developed. The deorientation theory and a new set of the parameters of polarimetric scattering targets are developed for terrain surface classification. The MPA (mapping and projection algorithm) technique of computer simulation for POL-SAR image of complicated natural scene is developed. The MPA is further developed to simulation of bistatic POL-SAR images. Multi-aspect SAR images are employed for automatic reconstruction of three-dimensional objects. Making use of the Mueller matrix solution and morphological processing, the digital elevation mapping of the earth surface is inverted from a single-pass POL-SAR image data. Two-threshold expectation maximum and Markov random field algorithms are studied to make automatic change detection from multi-temporal SAR images over the urban area and some earthquake regions. The Mueller matrix at P band with the Faraday rotation is also studied and recovered. Inversion of multi-parameters of terrain canopy surface is also inverted. The algorithm of phase unwrapping of interferometric SAR (INSAR) is studied. The probability density functions of multi-look four Stokes parameters are derived. Some POL-SAR applications, such as ship detection and moving target refocusing etc., are also included.

Part 2 deals with the vector radiative transfer(VRT) theory for inhomogeneous scatter media. The VRT takes account of multiple scattering, emission and propagation in random scatter media, and quantitatively leads to insights of elucidating and understanding EM wave-terrain surface interaction. Meanwhile, it is extensively applicable to carrying out data interpretation and validation, and to solving the inverse problem, e. g. iteratively, physically or statistically. In this part, iterative solutions of multiple scattering and emission from inhomogeneous dense scatter media, e. g. snowpack, and inhomogeneous multi-layers non-spherical scatter media, e. g. vegetation canopy, are discussed. Three-dimensional VRT equation (3D-VRT) for spatially inhomogeneous random scatter media for high resolution observation is also investigated. The Mueller matrix solution for a pulse wave incidence upon layered media of random non-spherical scatterers is developed. It has been applied to several issues, such as detecting lunar subsurface, monitoring and early warning the debris flow and landslides.

Great amount of remote sensing data and images in temporal and spatial scales presents a challenge how to quantitatively extract the information from data-image and make new knowledge based on the information. Part 3 devotes to data validation from satellite-borne microwave remote sensing, e. g. SSM/I, AMSR-E, FY etc. The overall reviews of Chinese FY and HY satellite remote sensing, and the state 973 project "Theory and application for retrieval and fusion of spatial and temporal quantitative information of complex natural environment" are presented. Described by VRT and characteristic indexes e. g. polarization, scattering and anomalous one, the terrain surface moisture mapping, draught and flooding, snow-frost, sandstorm and desertification etc. , based on multi-year passive microwave remote sensing, are studied. Some natural algorithms such as genetic algorithm, artificial neural network, and Getis statistics etc. are applied to parameter retrievals. Correlations of active SAR and passive SSM/I observations over snowpack and oceanic surfaces are also demonstrated. Data fusions of Radarsat SAR and DMSP SSM/I for monitoring sea ice, and Landsat ETM+ and ERS-2 SAR for classification of urban terrain surfaces are studied.

Part 4 deals with computational electromagnetics, especially for composite scattering of a target presence on or above a randomly rough surface. It includes the generalized forward-backward method with the spectral accelerate algorithm (GFBM-SAA), the hybrid analytic Kirchhoff and numerical moment method (KA-MoM), the finite element method (FEM) with DDM (domain decomposition method) for large scale problem and FEM-TLQSA (two level quasi-stationary algorithm) for the Doppler spectrum of flying target over rough surface, the finite difference in time domain (FDTD) method for calculation of near-far fields from 3D target-rough surface etc. Bidirectional analytic ray tracing (BART) approach is developed for numerical calculation of scattering from 3D complex electric large target over rough surface. Using the technique of step-frequency radar, 3D imaging and reconstruction of a complex target on rough surface is then presented.

China had successfully launched its first lunar exploration satellite Chang E-1(CE-1) on October 24, 2007. Part 5 presents the research works on the modeling, data-image simulation and data validation for lunar exploration in both passive/active microwave remote sensing. As the first part, the works on Chinese Chang E(CE-1) lunar program, including theoretical model for brightness temperature simulation ($T_b$) of lunar surface media, CE-1 data validation and retrieval of lunar regolith layer thickness from multi-channel CE-1 $T_b$ data, and evaluation of global inventory of Helium-3 in lunar regolith, are reported. As the second section, scattering modeling and numerical SAR image simulation of the randomly cratered lunar surface, and high frequency(HF) radar range echoes from lunar surface-subsurface structures are presented.

I would like to acknowledge the collaborations with my colleagues and graduate students. They are: Huang Xingzhong, Xu Feng, Ye Hongxia, Fa Wenzhe, Cao Guangzheng, Kuang Lei, Wei Zhiqiang, Chen Hao, Ding Rui, Gong Xiaohui, Chang Mei, Liang Zhichang, Zhang Nanxiong, Chen Fei, Luo Ling, Dai Eryan, Qi Renyuan, Yan Fenghua, Wang Dafang, Dai Junwen, and postdoctorals Li Zhongxin, Liu Peng, Han Zheng, Peng Jing.

As a summary work in my research life during these decades, it is my great pleasure and honor to present these two-volume books to the colleagues and graduate students.

# 前　言

本书作为“自然介质电磁散射与辐射传输信息”的第二卷，选自我2001～2010年期间在国际学术刊物上发表的部分学术论文。其第一卷包括1983～2000年间的工作已由科学出版社在2000年出版。这两卷书包括了我在近30年里在电磁散射、辐射传输与空间微波遥感的主要研究工作。特别在本卷中包括了我作为国家重点基础研究计划973项目“复杂自然环境时空定量信息与融合处理的理论与应用”首席科学家时期我本人发表的一些论文。这些工作包含了极化散射与合成孔径雷达(SAR)遥感信息、复杂自然介质矢量辐射传输VRT、星载微波遥感数据验证、目标与环境复合电磁散射建模数值模拟、月球微波遥感五个方面的研究成果。

我的研究生黄兴忠、徐丰、叶红霞、法文哲、曹广真、匡磊、魏志强、陈昊、丁锐、宫晓惠、常梅、梁子长、张南雄、陈扉、罗霖、戴尔燕、戚任远、颜锋华、王大芳、戴俊文，博士后李中新、刘鹏、韩震、彭静在这些研究工作中做出了重要的贡献。

本书第一部分建立参数化建模的自然地表极化散射解与极化SAR信息理论，形成理论建模、散射辐射模拟、成像模拟、反演重构的微波遥感信息正演模拟与特征反演重构链。

提出了从随机非球形散射粒子、随机粗糙面的自然介质层电磁散射理论建模，获得全极化散射的Mueller矩阵解；提出全极化测量中散射特征矢量去取向理论，定义了新参数组及其地表新分类谱，实现对SAR观测地表的新分类方法；用参数化建模与映射投影算法(MPA)，实现复杂场景的SAR图像的模拟；进一步地，研究了新兴的双站SAR和极化分析，提出了双站SAR成像模拟和双站基转换的分析方法；用多方位SAR实现了三维建筑目标群的自动重构与立体重建的方法；提出用单次极化SAR图像对地面高程的反演方法；提出双阈值期望极大化与空间自相关Markov随机场(2EM-MRF)从多时相SAR图像自动识别散射差值“增强、减弱与不变”三类区域变化；研究了全极化P波段SAR的Faraday旋转(FR)效应，可以从FR后全极化测量反演无FR的全极化数据。极化干涉SAR(INSAR)的相位解缠问题进行了讨论。也研究了多视四个Stokes参数的统计解析分布，也讨论了一些极化SAR在海面舰船识别、桥高检测等方面的应用研究。

第二部分研究复杂自然介质矢量辐射传输理论(VRT)。

极化电磁波能量的散射、吸收与传输VRT是空间遥感的基础理论，空间遥感技术的发展促进和深化了VRT的发展。本部分讨论了三维VRT理论及其数值求解；非均匀分层、非球形散射粒子植被理论建模、密集散射元的非均匀积雪层理论建模的VRT理论；提出分层散射地表脉冲雷达的VRT的Mueller矩阵解；并特别提出了用VHF雷达对泥石流与滑坡的检测与预警技术。

第三部分讨论星载微波遥感数据验证的理论与方法。

综述了我国星载风云气象卫星与海洋卫星微波遥感的发展、作者主持的国家973项目“复杂自然环境时空定量信息获取与融合处理的理论与应用”的研究成果。以VRT为基础，提出散射与极化特征指数、异常特征指数等；对在轨SSM/I、AMSR-E、风云FY等星载微波遥感器数据进行特征事件试验与数据验证反演，如:植被生物量、土壤湿度、沙暴、干旱、洪涝、积雪、冰冻、海冰、降雨等典型事件特征物理参数的反演和人工神经网络(ANN)、遗传算法等自然计算的遥感参数特征重构，也讨论了城市环境红外与微波多源遥感信息融合及其应用研究的新方法。

第四部分讨论体目标与随机粗糙面共存时复合电磁散射的理论建模与数值计算方法。

在低掠角、低空、三维、电大、目标环境耦合等条件下，实现多种复杂海况与下视雷达监测条件变化时风驱粗糙海面杂波与船目标回波共存时双站与单站散射的数值模拟。其中包括：结合谱加速法的前后向迭代 GFBM/SAA 方法、解析与数值混合的 KA-MoM 方法、有限元 FEM 数值方法、风驱海面上运动目标散射的双级准静态方法研究 Doppler (DP) 频谱、起伏海面上电性特大三维目标船散射的双向解析射线跟踪方法(BART)、步进频率雷达对电性特大三维目标三维散射成像与目标特征重构、目标与粗糙面近场远场 FDTD 方法等，也讨论了手征介质与异向介质散射问题。

第五部分讨论中国探月工程微波探月的理论建模、反演、“嫦娥一号”数据验证与雷达成像研究工作。

提出中国“嫦娥一号”绕月计划多通道微波辐射计的月面分层介质微波辐射的建模模拟、分层物理温度与月壤层厚度反演、氦 3 含量估算、嫦娥绕月微波辐射数据验证与分析。也研究了环形山月球表面 SAR 成像模拟，雷达探测仪对月球分层介质的高频探测成像的理论与方法。

本文集论文是我近十年来研究工作的归纳，也映衬了我近十年的人生踪迹。

感谢 陈芳允、吕保维、陈述彭 、周秀骥、匡定波、黄宏嘉、林为干、朱中梁、侯朝焕、吕达仁、杨福家、童庆禧、杨玉良、周国治、胡文瑞等诸位先生多年来对我的推荐、鼓励与支持。

感谢在我学习工作中一些重要时刻给予我帮助与支持的徐冠华、刘盛纲、干福熹、姜景山、林海、秦瑜、吴季等诸位先生。

我也十分高兴地回忆在国家 973 项目中与陈洪滨、卢乃锰、韩崇昭、李新、张万昌、王超等同行专家的紧密合作。

中华文明的全面复兴与中国的和平崛起，是近 200 年来中华儿女志士仁人梦寐以求的伟大理想。在祖国命运发生根本变化的 1978 年，我奉考中国科学院大气物理研究所周秀骥先生的微波遥感研究生，遂即录取为首批公派赴美研究生留学。在美国麻省理工学院(MIT)，师从 J. A. Kong 教授、D. H. Staelin 教授。1987 年学成归来 20 多年寒暑春秋，我无一日懈怠，竭诚尽责，正己无怨。我历经上海中学、北京大学、中国科学院北京研究生院、美国麻省理工学院最好的教育，各门学科成绩优秀。在本书涵盖的 5 个研究领域，我为中国在电磁散射辐射传输与空间微波遥感信息基础研究的发展做出了贡献，也对国际该领域的研究进展与 IEEE GRSS 的发展做出了贡献。无愧无悔，夫复何求？

岁月荏苒，不知老之将至。“冯唐易老，李广难封。……宁移白首之心?”，“我不希荣，何忧乎利禄；我不兢晋，何畏乎仕宦”。立德立功立言是中华志士仁人的历史传统，我当追随之而无上荣光乎。

# Contents

## Part 1 Polarimetric Scattering and SAR Image Information


Polarimetric Scattering Indexes and Information Entropy of the SAR Imagery for Surface Monitoring …… 3
Statistics of Four Stokes Parameters in Multi-look Polarimetric Synthetic Aperture Radar (SAR) Imagery …… 7
Terrain Topography Inversion Using Single-Pass Polarimetric SAR Image Data …… 17
Automatic Detection of Change Direction of Multi-temporal ERS-2 SAR Images Using Two-Threshold EM and MRF Algorithms …… 28
Automatic Detection of Terrain Surface Changes after Wenchuan Earthquake, May 2008, from ALOS SAR Images Using 2EM-MRF Method …… 36
Analysis of the Effects of Faraday Rotation on Space-borne Polarimetric SAR Observation at P Band … 41
Deorientation Theory of Polarimetric Scattering Targets and Application to Terrain Surface Classification …… 49
Multiparameters Inversion of a Layer of Vegetation Canopy over Rough Surface from the System Response Function Based on the Mueller Matrix Solution of Pulse Echoes …… 63
Imaging Simulation of Polarimetric SAR for a Comprehensive Terrain Scene Using the Mapping and Projection Algorithm …… 75
Automatic Reconstruction of Buildings Objects from Multiaspect Meter-Resolution SAR Images …… 91
Three-Dimensional Stereo Reconstruction of Buildings Using Polarimetric SAR Images Acquired in Opposite Directions …… 109
Calibration and Validation of a Set of Multi-Aspect Airborne Polarimetric Pi-SAR Data …… 114
Imaging Simulation of Bistatic Synthetic Aperture Radar (SAR) and Its Polarimetric Analysis …… 124
Raw Signal Processing of Stripmap Bistatic Synthetic Aperture Radar …… 140
Phase Unwrapping for SAR Interferometry Based on an Ant Colony Optimization Algorithm … 152
Multiple Patches and Center Expansion Algorithms for Phase Unwrapping of InSAR Images with Dense Residues …… 167


## Part 2 Vector Radiative Transfer of Complex Media


Iterative Solution of Multiple Scattering and Emission from Inhomogeneous Scatter Media …… 179
Iterative Inversion from the Multi-Order Mueller Matrix Solution of Vector Radiative Transfer Equation for a Layer of Random Spheroids …… 185
Inversion of Scattering from a Layer of Rondom Spheroids Using Iterative Solutions of the Scalar Radiative Transfer Equation …… 194
An Approach of the Three-Dimensional Vector Radiative Transfer (3D-VRT) Equation for Inhomogeneous Scatter Media …… 202

Iterative Inversion of Canopy Parameters and Surface Moisture Using the Multi-Order Mueller Matrix Solution of the Vector Radiative Transfer Equation ····· 208
Scattering and Emission from Inhomogeneous Vegetation Canopy and Alien Target Beneath by Using Three-Dimensional Vector Radiative Transfer (3D-VRT) Equation ····· 215
Iterative Approach of High-Order Scattering Solution for Vector Radiative Transfer of Inhomogeneous Random Media ····· 229
Polarimetric Backscattering and Shift of Polarization Angle from Random Chiral Spheroids ····· 241
Scattering Simulation for Inhomogeneous Layered Canopy and Random Targets Beneath Canopies by Using the Mueller Matrix Solution of the Pulse Radiative Transfer ····· 256
Retrievals of Underlying Surface Roughness and Moisture from Polarimetric Pulse Echoes in the Specular Direction through Stratified Vegetation Canopy ····· 266
Temporal Mueller Matrix Solution for Polarimetric Scattering from Inhomogeneous Random Media of Non-spherical Scatterers ····· 273
Monitoring and Early Warning the Debris Flow and Landslides Using VHF Radar Pulse Echoes from Layering Land Media ····· 286

## Part 3 Modeling and Data Validation of Satellite-Borne Microwave Remote Sensing

Advancement of Chinese Meteorological Feng Yun (FY) and Oceanic Hai Yang (HY) Satellite Remote Sensing ····· 295
Theory and Application for Retrieval and Fusion of Spatial and Temporal Quantitative Information from Complex Natural Environment ····· 313
A Genetic Algorithm to Simultaneously Retrieve Land Surface Roughness and Soil Wetness ····· 328
Monitoring Sandstorms and Desertification in Northern China Using SSM/I Data and Getis Statistics ····· 335
Monitoring Flooding of the Huaihe River, China, in Summer 2003 Using Characteristic Indeces Derived from SSM/I Multitemporal Observations ····· 343
Suspended Sediment Concentrations in the Yangtze River Estuary Retrieved from the CMODIS Data ····· 348
A Hybrid Algorithm of the BP-ANN/GA for Classification of Urban Terrain Surfaces with Fused Data of Landsat ETM+ and ERS-2 SAR ····· 356
A Change Detection Algorithm for Terrain Surface Moisture Mapping Based on Multi-Year Passive Microwave Remote Sensing (Examples of SSM/I and TMI Channels) ····· 369
Detection of Snow and Frost in Southern China, January 2008 Using AMSR-E Scattering and Polarization Indexes ····· 376
Data Validation of Chinese Microwave FY-3A for Retrieval of Atmospheric Temperature and Humidity Profiles during Phoenix Typhoon, 2008 ····· 386
Automatic Detection of Main Road Network in Dense Urban Area Using Microwave SAR Images ····· 399
An Unbiased Algorithm for Detection of Curvilinear Structures in Urban Remote Sensing Image ····· 407

An Algorithm for Ship Wake Detection from the Synthetic Aperture Radar Images Using the Radon Transform and Topographical Image Processing ····· 426
An Improved Minimum Entropy Method for Refocusing the Moving Target Image in the Synthetic Aperture Radar Observation ····· 431

## Part 4 Computational Electromagnetics of Scattering from Randomly Rough Surface and Volumetric Objects

Reconstruction of Roughness Profile of Fractal Surfaces from Scattering Measurement at Grazing Incidence ····· 439
Simulation of Scattering from Complex Rough Surface at Low Grazing Angle Using the GFBM/SAA Method ····· 444
Bistatic Scattering and Transmitting through Fractal Rough Dielectric Surface Using FBM/SAA Method ····· 449
Numerical Simulation of Bistatic Scattering from Fractal Rough Surface Using the Forward/Backward Iterative Method ····· 470
Bistatic Scattering and Transmitting through a Fractal Rough Surface with High Permittivity Using the PBTG-FBM/SAA Method ····· 487
Numerical Simulation of Radar Surveillance for the Ship Target and Oceanic Clutters in Two-dimensional Model ····· 492
Numerical Simulation of Scattering from Fractal Rough Surface in the Finite Element Method ··· 498
Numerical Simulation for Bistatic Scattering from a Target at Low Altitude over Rough Sea Surface under EM Incidence at Low Grazing Angle by Using the Finite Element Method ····· 505
The Finite Element Method with Domain Decomposition for Electromagnetic Bistatic Scattering from the Comprehensive Model of a Ship on and a Target above Large-Scale Rough Sea Surface ··· 511
Numerical Simulation of the Doppler Spectrum of a Flying Target above Dynamic Oceanic Surface by Using the FEM-DDM Method ····· 518
An FEM Approach with FFT Accelerated Iterative Robin Boundary Condition for Electromagnetic Scattering of a Target with Strong or Weak Coupled Underlying Randomly Rough Surface ····· 526
Parameterization of Tapered Incident Wave for Electromagnetic Scattering Simulation from Randomly Rough Surface ····· 534
Polarimetric Scattering from a Layer to Spatially Oriented Metamaterial Small Spheroids ····· 537
Fast Iterative Approach to Difference Scattering from the Target above a Rough Surface ····· 544
A Hybrid Analytic-Numerical Algorithm of Scattering from an Object above a Rough Surface ··· 551
Bistatic Scattering from a Three-Dimensional Object over a Randomly Rough Surface Using the FDTD Algorithm ····· 557
A Hybrid KA-MoM Algorithm for Scattering from a 3-D PEC Target above a Dielectric Rough Surface ····· 567
Analytical Iterative Algorithm for Fast Computation of Scattering from Multiple Conductive Cylinders and the Image Reconstruction ····· 582
Dual GPOF /DCIM for Fast Computation of the Sommerfeld Integrals and Electromagnetic Scattering from an Object Partially Embedded in Dielectric Half-Space ····· 589

Bidirectional Analytic Ray Tracing for Fast Computation of Composite Scattering from An Electric-Large Target over Randomly Rough Surface ····· 596
Scattering and Image Simulation for Reconstruction of 3D PEC Objects Concealed in a Closed Dielectric Box ····· 607
Stochastic Functional Analysis of Propagation and Localization of Cylindrical Waves in a Two-Dimensional Random Medium ····· 619
Scattering Simulation and Reconstruction of a 3D Complex Target Using Downward- Looking Step-Frequency Radar ····· 637

## Part 5 Remote Sensing of Lunar Surface

Numerical Simulation of Polarimetric Radar Pulse Echoes from Lunar Regolith Layer with Scatter Inhomogeneity and Rough Interfaces ····· 651
Simulation of Brightness Temperature of Lunar Surface and Inversion of the Regolith Layer Thickness ····· 661
Quantitative Estimation of Helium-3 Spatial Distribution in the Lunar Regolith Layer ····· 674
SAR Imaging Simulation for an Inhomogeneous Undulated Lunar Surface Based on Triangulated Irregular Network ····· 683
An Inversion Approach for Lunar Regolith Layer Thickness Using Optical Albedo Data and Microwave Emission Simulation ····· 699
Simulation of Radar Sounder Echo from Lunar Surface and Subsurface Structure ····· 714
A Primary Analysis of Microwave Brightness Temperature of Lunar Surface and Chang-E 1 Multi-Channel Radiometer Observation and Inversion of Regolith Layer Thickness ····· 727
The Modeling Analysis of Microwave Emission from Stratified Media of Non-uniform Lunar Cratered Terrain Surface for Chinese Chang-E 1 Observation ····· 738
Global Inventory of Helium-3 in Lunar Regolith Estimated by Multi-Channel Microwave Radiometer on Chang-E 1 ····· 743
Diurnal Physical Temperature at Sinus Iridum Area Retrieved from Observations of CE-1 Microwave Radiometer ····· 748

**Publication List** ····· 757

# Part 1 Polarimetric Scattering and SAR Image Information


Polarimetric Scattering Indexes and Information Entropy of the SAR Imagery for Surface Monitoring ..... 3

Statistics of Four Stokes Parameters in Multi-look Polarimetric Synthetic Aperture Radar (SAR) Imagery ..... 7

Terrain Topography Inversion Using Single-Pass Polarimetric SAR Image Data ..... 17

Automatic Detection of Change Direction of Multi-temporal ERS-2 SAR Images Using Two-Threshold EM and MRF Algorithms ..... 28

Automatic Detection of Terrain Surface Changes after Wenchuan Earthquake, May 2008, from ALOS SAR Images Using 2EM-MRF Method ..... 36

Analysis of the Effects of Faraday Rotation on Space-borne Polarimetric SAR Observation at P Band ..... 41

Deorientation Theory of Polarimetric Scattering Targets and Application to Terrain Surface Classification ..... 49

Multiparameters Inversion of a Layer of Vegetation Canopy over Rough Surface from the System Response Function Based on the Mueller Matrix Solution of Pulse Echoes ..... 63

Imaging Simulation of Polarimetric SAR for a Comprehensive Terrain Scene Using the Mapping and Projection Algorithm ..... 75

Automatic Reconstruction of Buildings Objects from Multiaspect Meter-Resolution SAR Images ..... 91

Three-Dimensional Stereo Reconstruction of Buildings Using Polarimetric SAR Images Acquired in Opposite Directions ..... 109

Calibration and Validation of a Set of Multi-Aspect Airborne Polarimetric Pi-SAR Data ..... 114

Imaging Simulation of Bistatic Synthetic Aperture Radar (SAR) and Its Polarimetric Analysis ..... 124

Raw Signal Processing of Stripmap Bistatic Synthetic Aperture Radar ..... 140

Phase Unwrapping for SAR Interferometry Based on an Ant Colony Optimization Algorithm ..... 152

Multiple Patches and Center Expansion Algorithms for Phase Unwrapping of InSAR Images with Dense Residues ..... 167

# Polarimetric Scattering Indexes and Information Entropy of the SAR Imagery for Surface Monitoring*

Jin Ya-Qiu and Chen Fei

***Abstract*—The Mueller matrix solution and eigenanalysis of the coherency matrix for completely polarimetric scattering have been applied to analysis of the synthetic aperture radar (SAR) imagery. Copolarized and cross-polarized backscattering for any polarized incidence can be obtained. The polarization index is usually defined as a parameter to classify the difference between polarized scattering signatures from the terrain surfaces. In this paper, the eigenvalues of the coherency matrix and information entropy are derived to directly relate with measurements of the copolarized and cross-polarized indexes. Thus, it combines the Mueller matrix simulation, the information entropy of the coherence matrix, and two polarization indexes together and yields a quantitative evaluation for surface classification in the SAR imagery. This theory is applied to analysis of the AirSAR images and fields measurements.**

***Index Terms*—Entropy, polarimetric indexes, surface classification, synthetic aperture radar image.**

## I. Introduction

SYNTHETIC aperture radar (SAR) imagery technology is one of most important advances in spaceborne microwave remote sensing during recent decades. Completely polarimetric scattering from complex terrain surfaces can be measured [12]. Fully understanding and retrieving information from polarimetric scattering signatures of natural media have become a key issue for SAR remote sensing and its broad applications.

During recent years there has been extensive research on polarimetric scattering for SAR imagery [2]. Numerical simulation of polarimetric scattering from natural media via the Mueller matrix solution has been studied [3], [9]. The coherency matrix and eigenanalysis of information entropy have been studied for polarimetry of natural media in SAR imagery [1], [5].

To indicate the difference between vertically (vv) and horizontally (hh) copolarized backscatterings, the polarization index was usually defined to classify the polarized scattering signature from different natural media.

However, the entropy and eigenanalysis need full Mueller matrix measurement and have not been directly related with the backscattering signatures. In other words, how to present the entropy and eigenanalysis merely from backscattering measurement has not been demonstrated.

In this paper, the relationship between the entropy and copolarized, cross-polarized backscattering indexes is established. Thus, it can now combine the Mueller matrix solution, the entropy of the coherency matrix, and measurements of the polarization indexes together and yield a quantitative description of the natural media. As examples, this theory is applied to an AirSAR image and field measurements for surface monitoring and classification.

## II. Mueller and Coherency Matrices With Eigenanalysis

As a polarized wave $\overline{E}_{\rm inc}(\chi, \psi)$ is incident upon the natural media, the scattering field is written as

$$\begin{bmatrix} E_{\rm vs} \\ E_{\rm hs} \end{bmatrix} = \frac{e^{{\rm i}kr}}{r} \begin{bmatrix} F_{\rm vv} & F_{\rm vh} \\ F_{\rm hv} & F_{\rm hh} \end{bmatrix} \cdot \begin{bmatrix} E_{\rm vi} \\ E_{\rm hi} \end{bmatrix} \equiv \frac{e^{{\rm i}kr}}{r} \overline{\overline{F}} \cdot \overline{E}_{\rm inc}(\chi, \psi) \tag{1}$$

where the $2 \times 2$-D (dimensional) complex scattering amplitude function $\overline{\overline{F}}$ can be measured by the polarimetry. The incident polarization is indicated by the elliptic and orientation angles $(\chi, \psi)$. Using the Mueller matrix solution of vector radiative transfer equation [3], [9] and (1), the scattered Stokes vector (four Stokes parameters) can be obtained as

$$\overline{I}_s(\theta, \phi) = \overline{\overline{M}}(\theta, \phi; \pi - \theta_0, \phi_0) \cdot \overline{I}_i(\chi, \psi). \tag{2}$$

Making use of the Mueller matrix solution of vector radiative transfer theory, the theoretical model and numerical simulation of polarimetric scattering from the layering scatter media have been studied [6]. The Mueller matrix $\overline{\overline{M}}$ is constructed by the nondiagonal extinction matrix $\overline{\overline{\kappa}}_e$ and the functions $\langle F_{pq} F_{st}^* \rangle$, $p, q, s, t = v, h$. The copolarized and cross-polarized backscattering coefficients $\sigma_c$ and $\sigma_x$, polarization degree $m_s$ for scattered Stokes echo with partial polarization, and other functions can be numerically calculated.

In either the measurement or theoretical simulation, a key issue is to understand the scattering mechanism through the Mueller matrix solution. The Mueller matrix is a $4 \times 4$-D real matrix with complex eigenvalues and eigenvectors. To be physically realizable, this matrix must satisfy the Stokes criterion together with several other restrictive conditions [10]. Unfortunately, however, these restrictions do not have any direct physical interpretation in terms of the eigenstructure of the Mueller matrix. The coherency matrix $\overline{\overline{C}}$ is applied to the study of polarimetric scattering of SAR images [1], [5]. Define the scattering vector as

$$\overline{t} = \frac{1}{2} [F_{\rm vv} + F_{\rm hh}, F_{\rm vv} - F_{\rm hh}, F_{\rm vh} + F_{\rm hv}, i(F_{\rm vh} - F_{\rm hv})]^T \equiv \frac{1}{2} [A, B, C, iD]^T \tag{3}$$

* IEEE Transactions on Geoscience and Remote Sensing, 2002, 40(11): 2502-2506

This work was supported by the China State Key Basic Research Project 2001CB309401 and CNSF 49831060, 60171009.

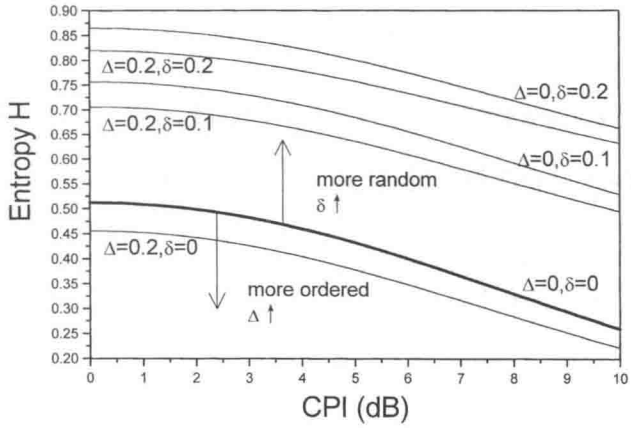


Fig. 1 Entropy $H$ versus index CPI with variations of $\Delta$ and $\delta$.

(8) from the full Mueller matrix solution. Then, the entropy $H$ of (7) is calculated using $P_i$ of (16)–(20). It can be seen that the function $P_1$ is related with the total vv and hh copolarized power $\sigma_{\rm hh}+\sigma_{\rm vv}$; $P_2$ is due to the difference between $\sigma_{\rm hh}$ and $\sigma_{\rm vv}$; and $P_3$ is due to depolarization $\sigma_{\rm hv}$. They are modulated by the media configuration and randomness via the parameters $\Delta$ and $\delta$. As the medium becomes more random or disordered, $\delta$ increases, and $\Delta$ approaches zero. Vice versa, as the medium becomes more ordered, $\delta$ decreases, and $\Delta$ increases. Thus, the relationship between the entropy $H$ and backscattering measurements $\sigma_{pq}(pq={\rm vv,hh,hv})$ is established.

Define the copolarized (CPI) and cross-polarized indexes (XPI), respectively, as

$$\text{CPI} \equiv 10\log_{10}(\sigma_{\rm hh}/\sigma_{\rm vv})\ (\text{dB}) \tag{21}$$

$$\text{XPI} \equiv \delta. \tag{22}$$

The question in Section II is answered that the entropy $H$ is directly related with backscattering indexes CPI and XPI via (16)–(22).

## IV. Demonstration With AirSAR Imagery

Fig. 1 presents the theoretical relationship between the entropy $H$ and index CPI with variations of the parameters $\Delta$ and $\delta$. The entropy $H$ is calculated by (16)–(20), i.e., via $\sigma_{\rm hh}$, $\sigma_{\rm vv}$, $\sigma_{\rm hv}$, and variations of $\Delta$ and $\delta$. It can be seen that as the medium becomes more random ($\delta$ increases) and CPI becomes smaller, $H$ will be increased. Vice versa, as the medium becomes more ordered and CPI becomes larger, $H$ will be decreased. The bold line in Fig. 1 is for the case of $\Delta=0$ and $\delta=0$. More randomness will shift $H$–CPI upward. Or vice versa, the ordered or less random medium will move $H$–CPI downward. The distance of the line $H$–CPI from this solid line indicates how much random the medium might be.

Fig. 2 presents an AirSAR image of total power of $\sigma_{\rm vv}$, $\sigma_{\rm hh}$, and $\sigma_{\rm vh}$ at the L-band over a Jack Pine area of Canada (near the Prince Albert National Park, about 103.33°W, 53.9°N). The image data from some typical areas such as the lake, an island surface, sparse trees, and thick forest (see the frames in the figure) are chosen, and their $H$, CPI, and XPI are compared.

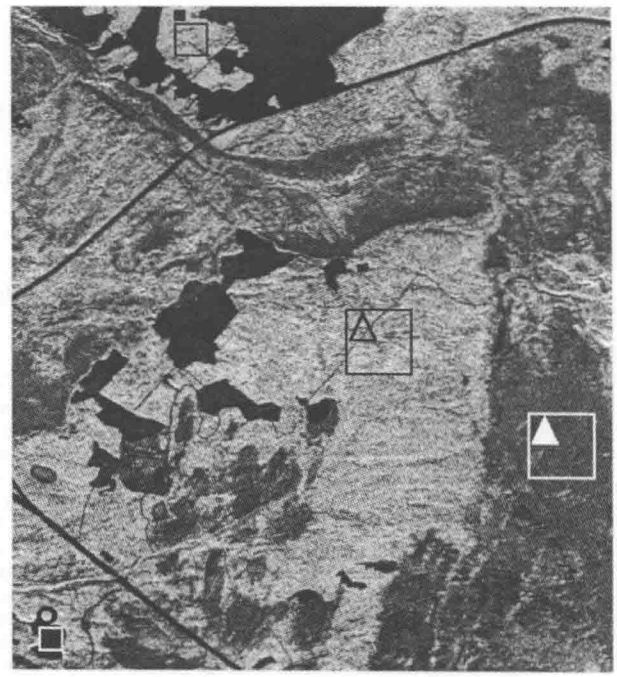

Fig. 2 AirSAR image of total power $\sigma_{\rm vv}$, $\sigma_{\rm hh}$, and $\sigma_{\rm vh}$ at L-band.

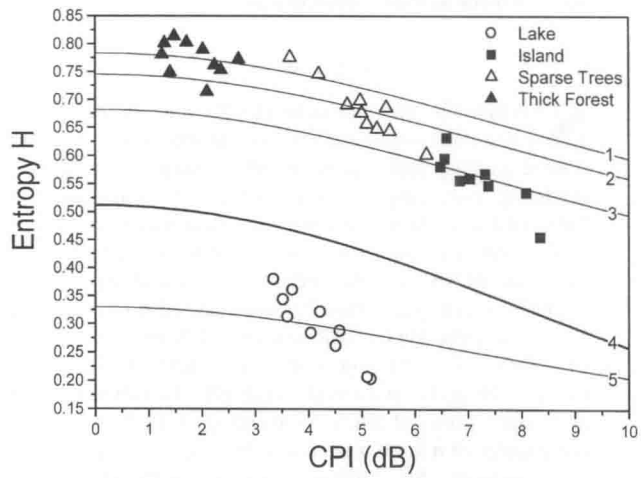


Fig. 3 Entropy $H$ and index CPI for surface classification from AirSAR data. Line 1: $\Delta=0.257$, $\delta=0.176$, Line 2: $\Delta=0.318$, $\delta=0.156$, Line 3: $\Delta=0.365$, $\delta=0.118$ Line 4: $\Delta=0$, $\delta=0$, Line 5: $\Delta=0.731$, $\delta=0.0265$.

To demonstrate the $H$–CPI relationship from the AirSAR imagery, Fig. 3 shows discrete points of the $H$–CPI from four regions of Fig. 2. The $H$ is first rigorously calculated by polarimetric data of the Mueller matrix, i.e., the eigenvalues of coherency matrix $\overline{\overline{C}}$ of (4). Using the AirSAR data $\sigma_{\rm vv}$, $\sigma_{\rm hh}$, $\sigma_{\rm vh}$, and the averaged $\delta$ in the respective region, the lines are calculated by (16)–(20) with appropriate $\Delta$ to match the center of discrete data. All $\delta$ and $\Delta$ are listed in the figure title. The bold line is for the case of $\Delta=0$ and $\delta=0$. The lines to match discrete data indicate how far the data in the region are from the case of $\Delta=0$ and $\delta=0$ and how random the media are. It can